PAPER • OPEN ACCESS

Micro-structured heat exchanger for cryogenic mixed refrigerant cycles

To cite this article: D Gomse *et al* 2017 *IOP Conf. Ser.: Mater. Sci. Eng.* **278** 012061

View the article online for updates and enhancements.

Related content

Micro-structured heat exchanger for cryogenic mixed refrigerant cycles

D Gomse[1,2]**, A Reiner**[1]**, G Rabsch**[3]**, T Gietzelt**[3]**, J J Brandner**[3]**,
S Grohmann**[1,2]

[1]Karlsruhe Institute of Technology, Institute of Technical Physics,
Hermann–von–Helmholtz–Platz 1, 76344 Eggenstein–Leopoldshafen, Germany
[2]Karlsruhe Institute of Technology, Institute of Technical Thermodynamics and Refrigeration,
Engler–Bunte–Ring 21, 76131 Karlsruhe, Germany
[3]Karlsruhe Institute of Technology, Institute of Micro Process Engineering,
Hermann–von–Helmholtz–Platz 1, 76344 Eggenstein–Leopoldshafen, Germany

E-mail: david.gomse@kit.edu

Abstract. Mixed refrigerant cycles (MRCs) offer a cost- and energy-efficient cooling method for the temperature range between 80 and 200 K. The performance of MRCs is strongly influenced by entropy production in the main heat exchanger. High efficiencies thus require small temperature gradients among the fluid streams, as well as limited pressure drop and axial conduction. As temperature gradients scale with heat flux, large heat transfer areas are necessary. This is best achieved with micro-structured heat exchangers, where high volumetric heat transfer areas can be realized. The reliable design of MRC heat exchangers is challenging, since two-phase heat transfer and pressure drop in both fluid streams have to be considered simultaneously. Furthermore, only few data on the convective boiling and condensation kinetics of zeotropic mixtures is available in literature. This paper presents a micro-structured heat exchanger designed with a newly developed numerical model, followed by experimental results on the single-phase pressure drop and their implications on the hydraulic diameter.

1. Introduction

In recent years, the application of MRCs as a reliable and efficient refrigeration method for high-temperature superconductors in cables, fault current limiters, etc. has been reviewed [1–3]. MRCs consist of a Linde-Hampson refrigeration cycle operated predominately in the two-phase region of wide-boiling mixtures. This enables low temperature gradients among the fluid streams in the main heat exchanger and thus an increased process efficiency [4]. As low temperature gradients necessitate large heat transfer areas, micro-structured heat-exchangers are well suited due to their high volumetric heat transfer areas.

In recent work, a correlation-based, numerical heat exchanger model has been presented, capable of calculating heat transfer and pressure drop of zeotropic fluid mixtures simultaneously along the length of the heat exchanger [5]. Utilising this model, a micro-structured heat exchanger was designed for future use in MRCs. The counter-flow heat exchanger was produced by diffusion welding of 60 micro-structured sheets (stainless steel grade 1.4571). A schematic representation of these metal sheets is presented in figure 1. Each sheet was structured by etching 50 parallel, S-shaped channels with 400 μm width, 200 μm depth and 20 cm length. Additionally, the sheets
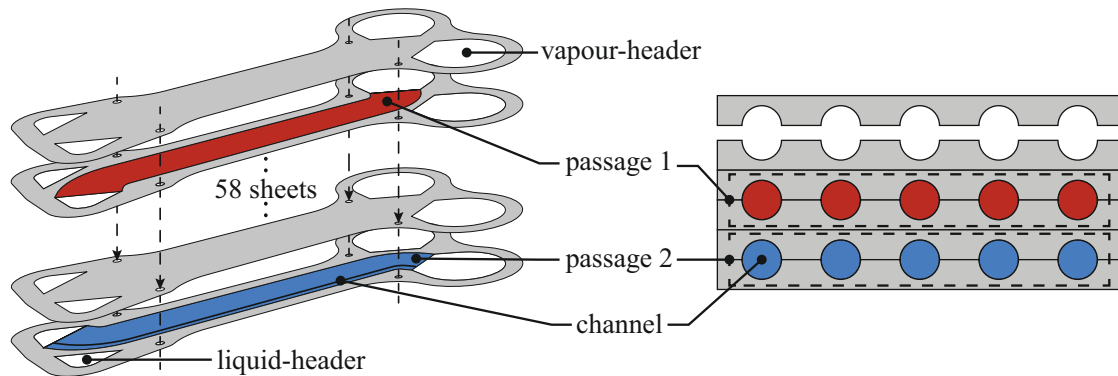
Figure 1. Schematic representation of a stack of micro-structured sheets.

comprise four positioning holes for sheet alignment and four cut out areas forming the headers. The sheets were stacked face-to-face prior to diffusion bonding to form round channels of 400 µm diameter. In total, the heat exchanger consists of two passages with 750 channels each. The vapour-headers are designed significantly larger than the liquid-headers to account for the density change due to evaporation and condensation. The area ratio was estimated following the design rule given by Kays et al. [6]:

$$\frac{A_\mathrm{l}}{A_\mathrm{v}} = \left[\left(\frac{\rho_\mathrm{l}}{\rho_\mathrm{v}} \right)^{0.5} \left(\frac{\pi}{2} \right) \right]^{-1} \tag{1}$$

where A depicts the cross-section area and ρ the fluid density.

Both isotropic wet-chemical etching and face-to-face stacking typically do not yield exact channel geometries. While isotropic etching tends to produce elliptical channels rather than perfectly circular ones [7], diffusion bonding of face-to-face stacked micro-structured sheets can lead to a parallel offset between the channels. Hence, the resulting channel geometry can differ significantly from the specified one. In order to assess the magnitude of this deviation, the single-phase laminar pressure drop is investigated at room temperature. Since the Poiseuille law provides an analytical solution for the pressure drop in the laminar flow regime, an accurate estimate of the effective hydraulic diameter can be derived.

The pressure drop model used to correlate the generated data and the influence of the manufacturing process on the channel geometry are described in section 2. The experimental procedure of the pressure drop measurements is presented in section 3. In section 4 the results are presented and discussed. Finally, the paper is summarised in section 5.

2. Theoretical framework
In this section, the equations used to model the single-phase pressure drop in the heat exchanger are outlined and the effect of the manufacturing steps on the channel geometry is discussed.

2.1. Pressure drop model
In general, the pressure drop is calculated by integrating

$$\frac{\partial p}{\partial z} = -\zeta \, \frac{\dot{m}^2}{2 \, \rho \, d_\mathrm{h}} \tag{2}$$

along the length of a channel. Here p depicts the pressure, z the axial position along the channel length, ζ the Darcy friction factor and $\dot{m}$ the mass flux. The hydraulic diameter d_h of the channel

can be derived from the cross-section area A and the circumference C:

$$d_{\mathrm{h}} = \frac{4\,A}{C}. \tag{3}$$

In the laminar flow regime the friction factor is defined by the Poiseuille law as

$$\zeta \;=\; \frac{64}{Re}, \tag{4}$$

$$Re \;=\; \frac{\dot{m}\,d_{\mathrm{h}}}{\eta} \tag{5}$$

where Re is the Reynolds number and η is the dynamic viscosity of the fluid.

For the two $45\,^\circ$ bends of the S-shaped channels, an equation derived by Hausen [8] based on data by White [9] is used to calculate the friction factor

$$\zeta_{\mathrm{bend}} = \zeta \left(0.0448 \left(\frac{Re}{\sqrt{\frac{2\,R}{d_{\mathrm{h}}}}} \right)^{0.6} + 0.805 \right) \tag{6}$$

where R is the radius of the bend.

The pressure drop at the entrance and exit of the heat exchanger core is calculated according to Kays et al. [6]:

$$\zeta_{\mathrm{in}} \;=\; 1 - \sigma^2 + K_{\mathrm{c}}, \tag{7}$$

$$\zeta_{\mathrm{out}} \;=\; 1 - \sigma^2 - K_{\mathrm{e}} \tag{8}$$

with

$$K_{\mathrm{c}} \;=\; 1.07 - 0.4\,\sigma, \tag{9}$$

$$K_{\mathrm{e}} \;=\; 1 - 2.67\,\sigma + \sigma^2 \tag{10}$$

where σ depicts the flow area ratio and K_{c} and K_{e} the contraction and expansion coefficients for laminar flow taken from figure 5-2 in Kays et al. [6].

The fluid properties of the test fluids, helium and air, were calculatd with REFPROP [10–12] using the local pressure and the average of inlet and outlet temperatures.

2.2. Channel geometry

In order to quantify the effect of the manufacturing process on the hydraulic diameter, three influences are discussed:

- wet-chemical etching,
- parallel offset of the micro-structured sheets and
- surface roughness of the channel walls.

The isotropic wet-chemical etching process typically yields elliptical rather than circular channels (cf. figure 2) [7]. The manufacturing tolerances of the etching process are specified with $\pm 60\,\mu\mathrm{m}$ and $\pm 30\,\mu\mathrm{m}$ for the channel width and height, respectively. This results in a $\pm 60\,\mu\mathrm{m}$ uncertainty of the hydraulic diameter.

The change in hydraulic diameter caused by a parallel offset x_{os} of two structured sheets stacked face-to-face is given by

$$d_{\mathrm{h,os}} = \frac{4\,A}{C + 2\,x_{\mathrm{os}}}. \tag{11}$$

As illustrated in figure 2, the hydraulic diameter is reduced due to an increase in circumference while the flow area remains constant. The diameter tolerance of the positioning hole for sheet alignment is given with $+80\,\mu m$. In case of a circular channel with a $400\,\mu m$ diameter, a parallel offset of $+80\,\mu m$ results in a reduction of the hydraulic diameter by $-45.2\,\mu m$.

On account of the small hydraulic diameters utilised in compact heat exchangers, the roughness introduced to the channel walls through etching can lead to high relative roughness values. Therefore, the surface roughness can influence the pressure drop even in the laminar flow regime. Kandlikar et al. [13] have proposed to consider roughness effects by modifying the flow diameter based on constrictions caused by the surface roughness. The constricted flow diameter $d_{\mathrm{h,cf}}$ is given by

$$d_{\mathrm{h,cf}} = d_{\mathrm{h}} - 2\epsilon \tag{12}$$

where ϵ is the average roughness height. Therefore, a typical worst case estimate of $5\,\mu m$ average roughness height reduces the hydraulic diameter by $-10\,\mu m$.

Considering all the effects mentioned above yields a hydraulic diameter of $400\,^{+\,60}_{-115.2}\,\mu m$.

3. Experimental method

A schematic representation of the experimental set-up used to investigate the pressure drop is shown in figure 3. The flow rate of the test medium (dry air or helium) is regulated with a hand valve. Before entering the test section, the temperature of the gas is controlled with a water bath. The gas temperatures up- and downstream of the heat exchanger (TI 1 & 2) are measured with a Pt-100 Class B platinum thermometer and a Endress+Hauser TMT84 temperature transmitter. The absolute pressure in the laboratory and the relative pressure before the heat exchanger (PI 3) are both determined with Endress+Hauser PMC731 pressure transmitters. Since each heat exchanger passage is equipped with only one pressure port at either the liquid- or vapour-header, the pressure drop of the heat exchanger core cannot be measured directly. Additionally, the liquid- and vapour-header are equipped with different diameter tubing. Therefore, the tubing pressure drop on the liquid- and vapour-side can each only be determined with passage 1 or 2, respectively. Endress+Hauser PMD235 differential pressure transmitters are used to measure the pressure difference between the up- and downstream pressure ports (PDI 4) and between either the upstream pressure port and the upstream header (PDI 5-1) or the downstream header and the downstream pressure port (PDI 5-2), depending on flow direction. In order to isolate the core pressure drop from the tubing pressure drop, the experimental values for the liquid- and vapour-side tubing are interpolated and subtracted from the PDI 4 data. The gas flow rate is
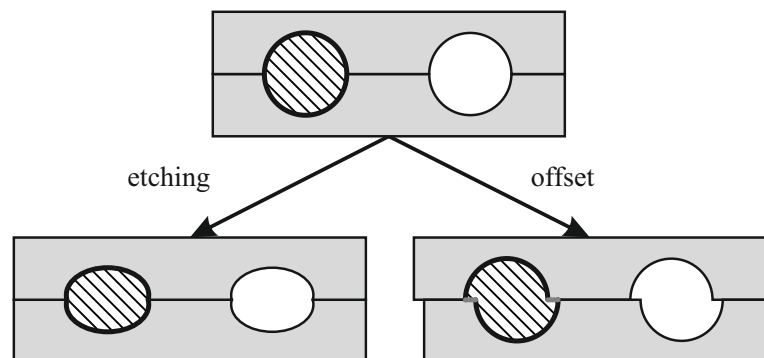
Figure 2. Schematic representation of the influence of isotropic etching and parallel offset on d_{h}.

determined with TetraTec laminar flow elements (50MH10-1 & 50MH10-2).

Each data point is the average of 100 measurements taken at a 5 Hz sampling rate. All uncertainties are given as expanded uncertainties according to the guide to the expression of uncertainty in measurement (GUM) [14], using both Type A and Type B contributions with a coverage factor of $k = 2$.

During the course of the experiments, the pressure drop of both heat exchanger passages is determined in either flow direction and with gaseous helium and air. Helium flow rates of $0.05 - 1\,\mathrm{g/s}$ and air flow rates of $0.25 - 4\,\mathrm{g/s}$ were achieved, resulting in Reynolds numbers of $10 - 250$ and $60 - 1100$, respectively.

4. Results and discussion

A comparison of the experimentally determined Darcy friction factors with Poiseuille's law (cf. equation 4) is depicted in figure 4. For this comparison, the effect of the 45° bends as well as the entrance and exit losses are subtracted from the experimental core pressure drop. The experimental data based on the nominal diameter exhibit a significant parallel offset from the prediction of laminar theory. This indicates that all data points correspond to the laminar flow regime, but the effective channel geometry deviates substantially from the specified one.

Figure 5 illustrates that the model under-predicts the experimental data by up to 65 %. In order to estimate the uncertainty of the predicted pressure drop, the ideal gas law is used to calculate the gas density and the pressure dependence of the gas viscosity is neglected. In this comparison, the uncertainty of the hydraulic diameter estimated in section 2.2, accounts for over 99 % of the error bars of the calculated pressure drop. The uncertainties due to temperature, pressure and mass flow measurements evaluate to only $0.0 - 0.7\,\mathrm{mbar}$, $0.1 - 1.8\,\mathrm{mbar}$ and $0.1 - 3.2\,\mathrm{mbar}$, respectively. This highlights the high degree of sensitivity of the pressure drop regarding the hydraulic diameter.

To account for the effects mentioned in section 2.2, effective hydraulic diameters for both passages are determined by fitting the pressure drop model to each individual experimental
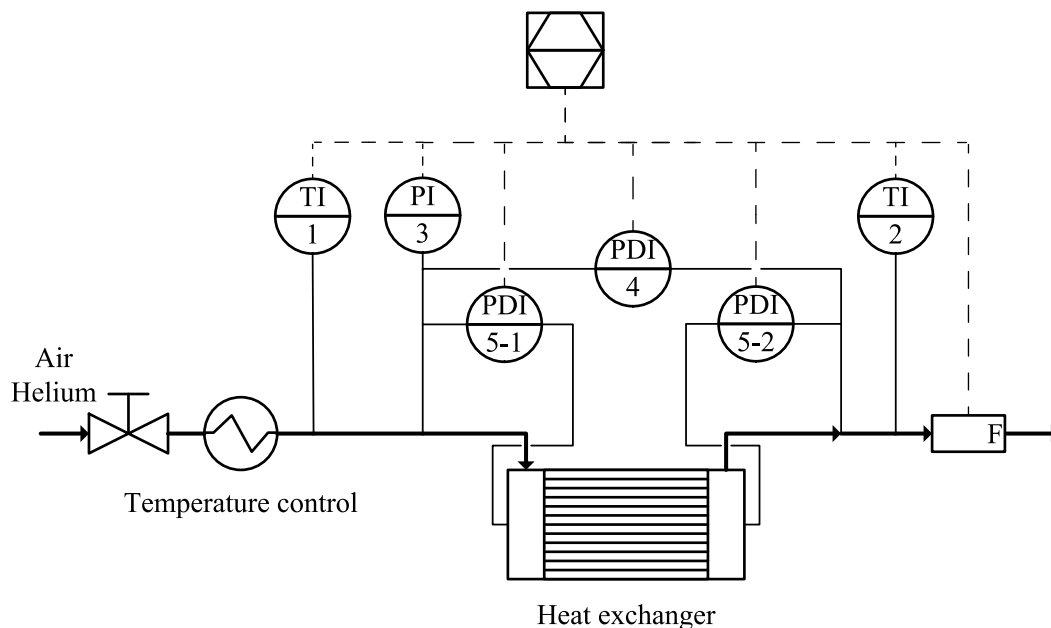
Figure 3. Schematic representation of the experiential set-up.
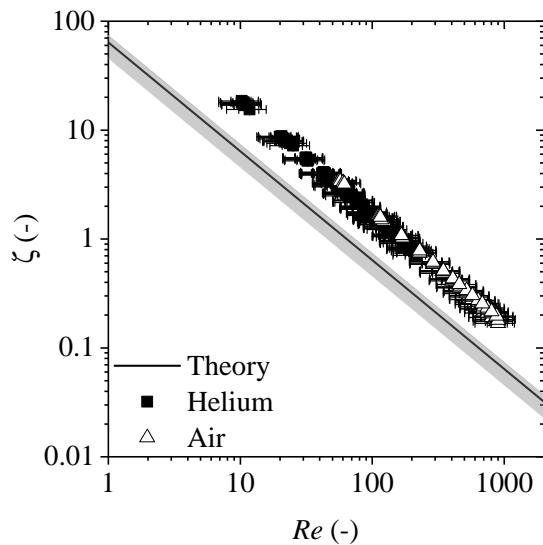
Figure 4. Comparison of experimental data with laminar theory; Darcy friction factor vs. Reynolds number (d_{h}=400 $^{+60}_{-115.2}$ µm).
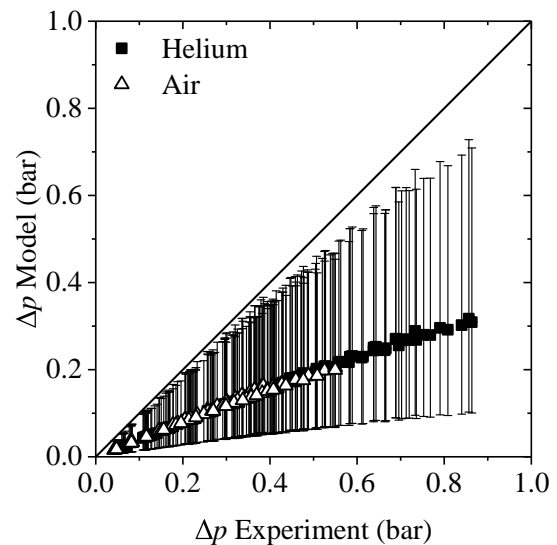
Figure 5. Comparison of experimental and calculated pressure drop values (d_{h}=400 $^{+60}_{-115.2}$ µm).
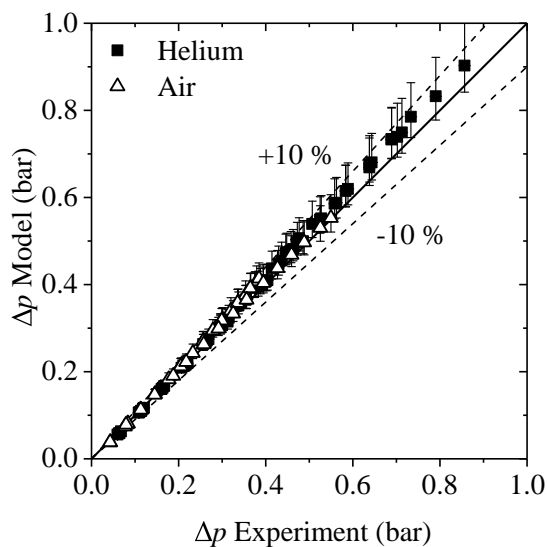
Figure 6. Comparison of experimental and calculated pressure drop values for passage 1 ($d_{\mathrm{h,1}}$=324.4 $^{+3.8}_{-6.3}$ µm).
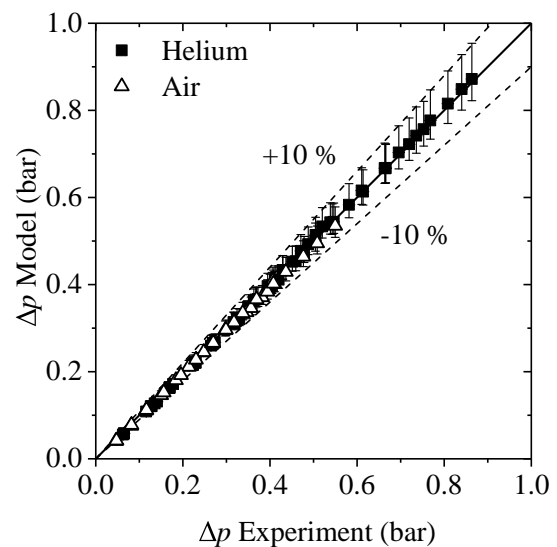
Figure 7. Comparison of experimental and calculated pressure drop values for passage 2 ($d_{\mathrm{h,2}}$=321.5 $^{+3.0}_{-5.0}$ µm).

value. This leads to a total of 198 individual hydraulic diameter values, 106 for passage 1 and 92 for passage 2. The distributions of these two datasets are best described by Weibull distributions (Pearson χ^2-, Kolmogorov-Smirnov- and Cramér-von Mises-tests yield P-values between 28 % and 57 %). The distributions predict effective hydraulic diameters of 324.4 $^{+3.8}_{-6.3}$ µm and 321.5 $^{+3.0}_{-5.0}$ µm for passages 1 and 2, respectively, with a 95 % confidence level. Using these effective hydraulic diameters, the model predicts the experimental pressure drop within a ± 10 % error band (cf.

figures 6 and 7). The combined uncertainty of the predicted pressure drop is still dominated by the hydraulic diameter, which accounts for $94.5 - 98.4\,\%$ of the uncertainty for passage 1 and $91.5 - 97.6\,\%$ for passage 2.

Additionally, it is interesting to note that, on average, the Poiseuille law makes up $97.4\,\%$ of the total pressure drop. The $45°$ bends and the entrance and exit effects account for only $1.5\,\%$ and $1.1\,\%$, respectively. As the Poiseuille law is of analytical origin, the plausibility of the effective hydraulic diameter can be assumed.

5. Summary and conclusions

In this paper a micro-structured heat exchanger for MRC applications is presented. The heat exchanger was designed with a correlation-based numerical model, capable of predicting heat transfer and pressure drop of zeotropic fluid mixtures. As an initial assessment of both heat exchanger and model performance, the single-phase pressure drop is determined with helium and air at room temperature. Experimental pressure drop values range from 0.05 to 0.9 bar with Reynolds numbers of 10–1100.

The experiments reveal a significant discrepancy between the specified and the actual channel geometry. Manufacturing tolerances, parallel offset of the micro-structured sheets and surface roughness are identified as the most significant influences on the hydraulic diameter. Employing effective hydraulic diameters of $324.4\,^{+3.8}_{-6.3}\,\mathrm{\mu m}$ and $321.5\,^{+3.0}_{-5.0}\,\mathrm{\mu m}$ for passage 1 and 2, respectively, the experimental data is predicted within a $\pm 10\,\%$ error band.

The effective hydraulic diameter provides the basis for future experimental investigations of heat exchanger and model performance. Since most heat transfer and pressure drop correlations are based on the hydraulic diameter, an accurate estimate of the hydraulic diameter is a precondition for a comparison between model and experiments in an MRC setup.

6. References

[1] Lee J, Hwang G, Jeong S, Park B J and Han Y H 2011 *Cryogenics* **51** 408–414
[2] Kochenburger T M, Grohmann S and Oellrich L R 2015 *Proceedings of the 25th International Cryogenic Engineering Conference and International Cryogenic Materials Conference 2014* **67** 227–232
[3] Narayanan V and Venkatarathnam G 2016 *Cryogenics* **78** 66–73
[4] Venkatarathnam G 2008 *Cryogenic mixed refrigerant processes* International cryogenics monograph series (New York: Springer)
[5] Gomse D, Kochenburger T M and Grohmann S 2017 *Journal of Heat Transfer* Submitted
[6] Kays W M and London A L 1998 *Compact heat exchangers* rep. ed. with corrections ed (Malabar, FL: Krieger Pub)
[7] Gatzen H H, Saile V and Leuthold J 2015 *Micro and Nano Fabrication* (Springer)
[8] Hausen H 1950 *Wärmeübertragung im Gegenstrom, Gleichstrom und Kreuzstrom* (Berlin, Heidelberg: Springer)
[9] White C 1929 *Streamline flow through curved pipes* vol 123
[10] Lemmon E W, Huber M L and McLinden M O 2013 Refprop: Nist standard reference database 23: Reference fluid thermodynamic and transport properties
[11] Vega D O O 2013 *A New Wide Range Equation of State for Helium-4* Ph.D. thesis Texas A&M University
[12] Lemmon E W, Jacobsen R T, Penoncello S G and Friend D G 2000 *Journal of physical and chemical reference data* **29** 331–385
[13] Kandlikar S G, Schmitt D, Carrano A L and Taylor J B 2005 *Physics of Fluids* **17**
[14] ISO/IEC Guide 98-3:2008 2008 Uncertainty of measurement – part 3: Guide to the expression of uncertainty in measurement Standard International Organization for Standardization Geneva, CH